2024 IEEE International Conference on Robotics and Automation (ICRA 2024)
May 13-17, 2024. Yokohama, Japan

# Soft Acoustic End-effector

Zhiyuan Zhang, Michael Koch, Daniel Ahmed*

***Abstract*—Acoustic techniques have been developed as multifunctional tools for various microscale manipulations. In prevalent design paradigms, a position-fixed piezoelectric transducer (PZT) is utilized to generate ultrasound waves. However, the immobility of the PZT restricts the modulation of the acoustic field's position and orientation, consequently diminishing the adaptability and effectiveness of subsequent acoustic micromanipulation tasks. Here, we proposed a miniaturized soft acoustic end-effector and demonstrated acoustic field modulation and microparticle manipulation by adjusting PZT position and orientation. The PZT is mounted on the end of a soft robotic arm that has three individual degrees of freedom and can be deformed in 3D space by inflating or deflating each chamber. Experiments showed that the soft acoustic end-effector can change the traveling direction of microparticles and modulate the location of a standing wave field. Our approach is simple, flexible, and controllable. We envision that the soft acoustic end-effector will facilitate multiscale acoustic manipulation in interdisciplinary applications, especially, for *in vivo* acoustic therapies.**

## I. Introduction

Acoustic techniques such as the acoustic traveling wave [1]–[3], acoustic standing wave [4]–[6], acoustic streaming [7], [8], acoustic tweezer [9], [10], and surface acoustic wave [11], [12] are widely utilized, portable, and multifunctional tools that can be employed for various manipulations of micro-objects in lab-on-chip systems [13], robotic actuators [14], [15], and medical applications [16]. A common design paradigm for acoustic micromanipulation devices consists of a glass slide with a position-fixed piezoelectric transducer (PZT) and a microcavity mounted on the slide [17]–[20]. It is widely recognized that a single PZT generates ultrasound waves exclusively in its polarization direction [21] and those waves attenuate significantly with propagating distance due to viscous attenuation by the medium [22], [23]. Therefore, a fixed PZT can only develop an acoustic field in a small area and the field's position and orientation cannot be easily adjusted by changing acoustic excitation parameters such as the excitation amplitude, frequency, and phase. Without degrees of freedom by which to adjust the pose of the PZT, the developed acoustic field is sluggish and the downline manipulation is monotonous. Consequently, position-fixed PZTs restrict the flexibility, effectiveness, and operation space of acoustic techniques.

* This project has received funding from the European Research Council (ERC) under the European Union's Horizon 2020 research and innovation programme grant agreement No. 853309 (SONOBOTS). Z.Z. acknowledges financial support from the China Scholarship Council (202006210065).

All authors are with the Acoustic Robotics Systems Laboratory, Institute of Robotics and Intelligent Systems, Department of Mechanical and Process Engineering, ETH Zurich, Säumerstrasse 4, CH-8803 Zurich, Switzerland. (e-mail: dahmed@ethz.ch).

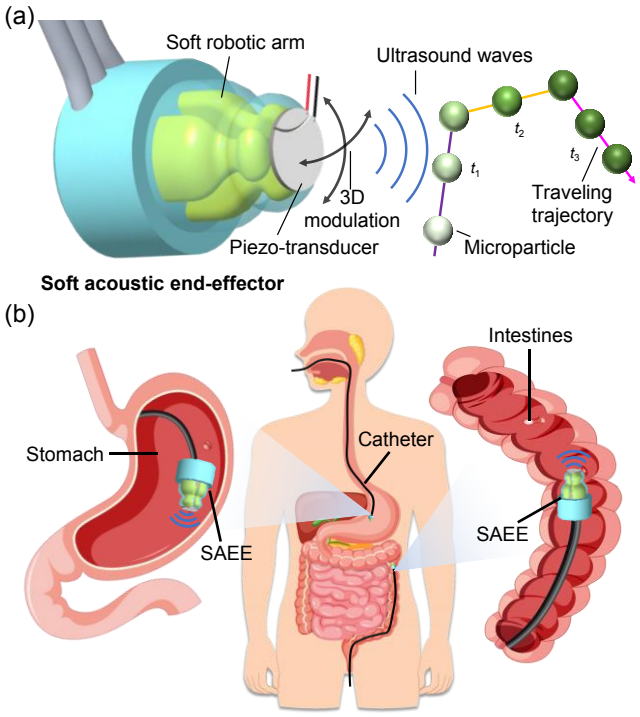


Fig. 1. Schematic of the soft acoustic end-effector (SAEE) and the potential *in vivo* applications. (a) PZT position and orientation are adjustable in 3D space by pneumatically actuating the soft robotic arm, allowing dynamic development of acoustic fields and manipulation of microparticles. (b) The SAEE guides a catheter to move through the stomach and intestines and enables pose adjustment of the PZT for multiple-angle acoustic therapies.

To date, several approaches allowing adjustment of acoustic fields have been studied. For example, transducer arrays that can be selectively excited to develop acoustic fields at different locations were designed [24], [25]. However, these devices are sophisticated and require complex programming. Researchers also used PZTs with special structures, like a spiral shape with variable spacing, to adjust the focus of an acoustic tweezer [26]. Whereas these devices lack the capacity for modulation in three-dimensional (3D) space. Moving the PZT in a plane can consequently move the acoustic field [27], but the method cannot be used in confined spaces and the fragile acoustic device may be damaged. Especially for *in vivo* applications, most existing acoustic field adjustment strategies are inferior due to limited acoustic penetration depth and difficulties in placing PZTs within the subject. Ultimately, precise 3D acoustic manipulation in complex and arbitrary environments remains challenging. A soft, flexible, and easy-to-operate method for acoustic field modulation is required.

Soft robots with light weight, high deformability, and excellent force output are promising candidates. Recently, a

millimeter-scale Delta robot has been reported for high-precision applications [28]. A miniature piezo parallel robot was studied for microscale gripping [29]. However, few works have been done on the micro-modulation of acoustic fields. Here, we report a miniaturized soft acoustic end-effector (SAEE) that addresses the necessities of modulating an acoustic field. In our approach, illustrated in Fig. 1, a PZT is mounted on the end of a soft robotic arm with three degrees of freedom. By inflating and deflating each gas chamber inside the arm, the position and orientation of the PZT can be adjusted in 3D space with properties that are simple, soft, compact, and precise. Then, by exciting the transducer with a high-frequency square signal, the developed acoustic field can be dynamically modulated and microparticles can be dexterously manipulated in a bulk liquid medium. The combination of a miniaturized soft robotic arm and microscale acoustic fields establishes a promising route for acoustic manipulation across multiple scales. We envision the SAEE for flexible and friendly human acoustic therapies. For example, the end-effector can maintain the conformable contact between the PZT and different skin curves for more effective acoustic coupling. Furthermore, Fig. 1b shows the long-distance *in vivo* navigation and therapies with the SAEE. The soft robotic arm can steer a catheter to move through the stomach and intestine, and then pose adjustment of the PZT offers multiple-angle acoustic micromanipulation.

## II. Methods and Materials

### A. Design and fabrication of the soft robotic arm

The soft robotic arm consists of a soft head with three individual gas chambers and a mini substrate. The two parts are then assembled into an entity. We engineered the gas chamber of the SAEE to include two subchannels, as illustrated in Fig. 2. This design ensures a flat end surface upon inflation, serving as an optimal mounting site for the PZT, and concurrently restricts the radial expansion of the soft head.

We developed finite element simulations of the soft head with different chamber designs to compare their deformation response. With the simulation model established by the commercial software Abaqus/Standard, the geometry body was defined as a 3D variability entity. The silicone rubber was defined as a hyperelastic material, which is described by the second-order Yeoh model of strain energy density function with the parameters of $C_1 = 0.11$, $C_2 = 0.02$ [30]. Next, the soft head was meshed using solid tetrahedral quadratic hybrid elements (C3D20H, Abaqus element type). The bottom surfaces of the models were fixed. Finally, ignoring the effects of gravity, a uniform pressure was applied to the entire internal surface of the gas chamber to simulate the process of inflating [31]. The thickness of the peripheral wall was set at $t_1$ = 1.0 mm and to achieve the function of strain-limiting, the intervening walls between the individual chambers were set at double thickness ($t_2$ = 2.0 mm). As shown in Fig. 2b to 2d and Movie S1, simulations demonstrated that both designs share the same deformation rules, i.e., when the three chambers are inflated at different pressures, the soft head bends to the side with lower pressure because of the asymmetrical resultant force; conversely, when the three chambers are inflated with the same pressure, the soft head extends axially due to the uniform resultant force. The soft head with the two-channel

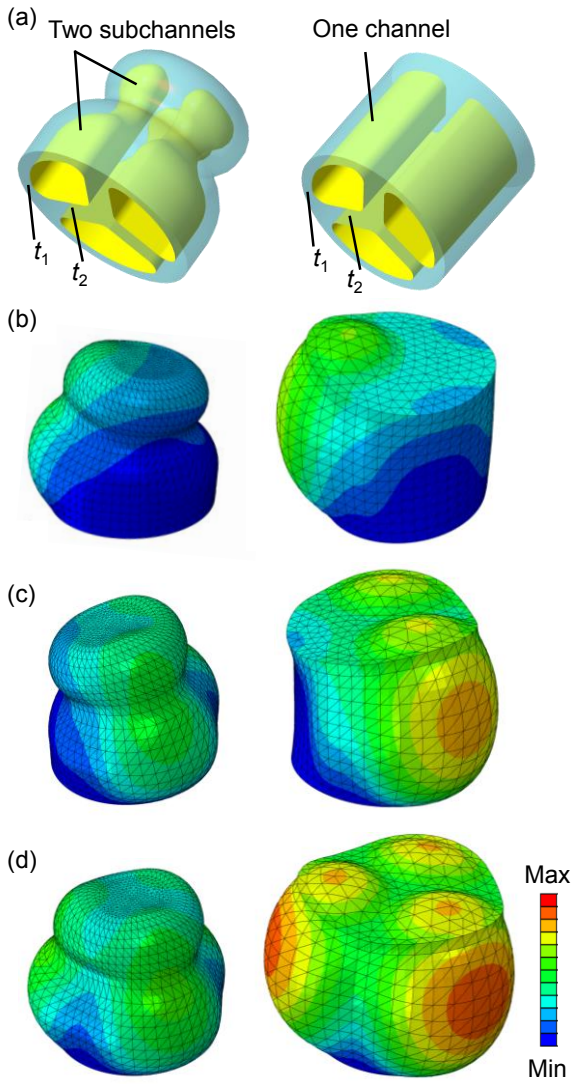


Fig. 2. Finite element simulations of soft robotic arms. (a) The arm with two-channel gas chambers and the arm with cylindrical gas chambers. Deformation of arms (b) when one gas chamber is inflated, (c) when two gas chambers are inflated, and (d) when three gas chambers are inflated. The input pressure of each chamber is 100 kPa. Colors denote the normalized deformation displacement. Grids denote the mesh of each arm.

design shows a similar bending angle and axial extension with the same driving pressure as the one having typical cylindrical gas chambers, implying a similar deformation efficiency. Importantly, the bulges on the upper surface and in the radial direction of our design are suppressed, which is crucial for precise PZT modulation within a small space.

The mini substrate was designed with micro pipes inside to align the pneumatic tubes to the gas chambers of the soft head, and was 3D printed with a transparent ABS resin (Acrylonitrile Butadiene Styrene). The soft head of the soft robotic arm was fabricated by standard mold-replica techniques [32], [33] using 3D printed molds (1.75 mm filament, EcoPLA) and liquid silicone rubber (Ecoflex 50, Smooth-on). Before molding, the casting molds were coated with trichlorosilane (1H,1H,2H,2H-perfluoro-octyl), a highly hydrophobic compound that acts as a mold release agent. The

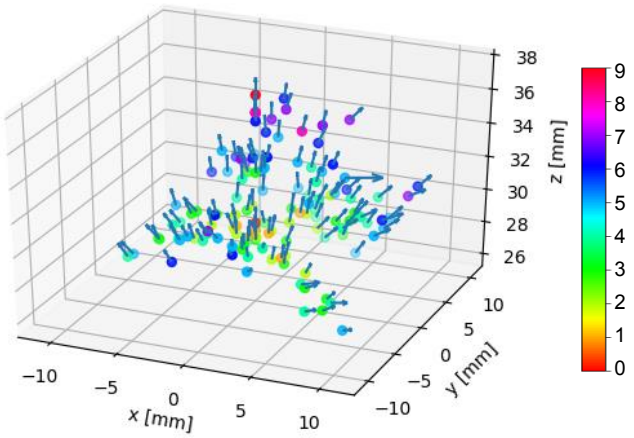


Fig. 3. Working space of the soft robotic arm. The color map denotes the total input gas volume to deform the arm to the target point from the initial pose.

mixed liquid rubber was vacuumed to remove small bubbles and then poured into the assembled molds. After curing, the soft head was removed from the molds and finally sealed and connected to the substrate with silicone glue.

### *B. Actuation and working space of the soft robotic arm*

Each gas chamber of the soft robotic arm can separately be inflated and deflated with compressed air, i.e., positive pressure and negative pressure actuating [34], [35], using a syringe that is connected to the pneumatic tubes. Applying a change of gas volume in each chamber respectively leads to a change of position and spatial orientation of the end of the soft robotic arm.

To estimate the working spacing of the soft robotic arm, it was placed on a millimeter graph paper and a tack was mounted on the end to show the normal vector of each shape. The gas volume range of the three syringes was given from $V = -1$ mL to 3 mL. In each test, the gas volume in one chamber was changed by 1 mL. The position of the tack tip and end were then measured. The normal vector of each deformed shape was calculated based on the collected data. Plotting the normal vector on a 3D coordinate system gives a representation of the working space of the soft robotic arm. As shown in Fig. 3, for changes in total volume $\Delta V = |V_1| + |V_2| + |V_3| = 0$ mL to 9 mL, the soft robotic arm is able to reach any angles in a spherical sector with polar angle $\theta \leq 5°$. Greater polar angle is only achievable in regions with azimuthal angle $\varphi \approx \{30°, 150°, 270°\}$, which is collected when only one chamber is inflated with maximum gas volume and the other two are deflated to the minimum gas volume. The results show that the soft robotic arm is a viable candidate for the subsequent acoustic micromanipulation.

### *C. Acoustic radiation force*

In this work, a circular PZT with dimensions 12 x 0.7 mm (Resonance frequency 5 MHz, Steminc) is utilized to generate acoustic traveling waves when excited by a high-frequency square signal. As the acoustic traveling waves propagate in liquid media, microparticles obstructing the wavefront are subjected to radiation forces. This acoustic radiation force consists of two components, a primary and a secondary radiation force. The primary radiation force arises from the interaction of the scattered wave from the particle with the underlying background wave. The secondary radiation force results from interactions of the scattered wave among nearby particles [36]. For spherical and uncompressible solid particles, the secondary radiation force is weak and thus can be ignored. In addition, as the dimension scales down to the micrometer, the buoyancy and gravity of particles reduce dramatically. As a result, the motion of particles will be dominated by the primary radiation force. Based on the gradient of the Gor'kov potential [37], for the particle with a radius $a$ much smaller than the wavelength, the time-averaged radiation force can be expressed as

$$F_{ar} = -\frac{4\pi}{3} a^3 \nabla \left[ f_1 \frac{1}{2\rho_0 c_0^2} \left\langle p_{in}^2 \right\rangle - f_2 \frac{3}{4} \rho_0 \left\langle v_{in}^2 \right\rangle \right], \tag{1}$$

$$f_1 = 1 - \tilde{k}, \text{ with } \tilde{k} = \frac{k_p}{k_0}, \tag{2}$$

$$f_2 = \frac{2(\tilde{\rho} - 1)}{2\tilde{\rho} + 1}, \text{ with } \tilde{\rho} = \frac{\rho_p}{\rho_0}, \tag{3}$$

where $p_{in}$, and $v_{in}$ are the incident acoustic pressure and incident acoustic velocity, respectively; $f_1$ and $f_2$ are dimensionless scattering coefficients; $\rho_0$, $\rho_p$ denote the density of the liquid and particle, respectively; $k_0$, $k_p$ denote the compressibility of the liquid and particle, respectively. During moving, the particle also subject to the Stokes' drag

$$F_d = 6\pi\eta a u, \tag{4}$$

where $\eta$ is the dynamic viscosity of the liquid and $u$ is the particle velocity.

Therefore, microparticles can be used to reveal the invisible acoustic field. In a traveling wave field, particles are pushed away from the PZT and move perpendicular to the PZT, due to the traveling wave mainly propagates perpendicular to the PZT. The moving direction of particles can be adjusted by changing the orientation of the PZT. On the other hand, as the traveling waves encounter an acoustic hard wall, the wave can be reflected to develop a standing wave field between the PZT and the wall. In the following, pressure nodes and antinodes are developed and solid particles in the field will be aligned and trapped to the node because of a positive acoustic contrast factor

$$\phi(\tilde{k}, \tilde{\rho}) = \frac{1}{3}\left[ \frac{5\tilde{\rho} - 2}{2\tilde{\rho} + 1} - \tilde{k} \right]. \tag{5}$$

As the orientation of the PZT changes, the standing wave field can be dynamically modulated and visualized by the changing particle patterns. Detailed acoustic radiation force analysis and microparticle behavior in both acoustic traveling wave field and acoustic standing wave field were described in

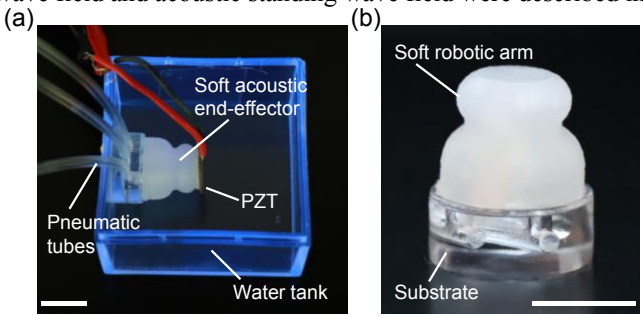


Fig. 4. Soft acoustic end-effector.(a) Experimental setup and (b) a prototype of the SAEE. Scale bar, 10 mm.

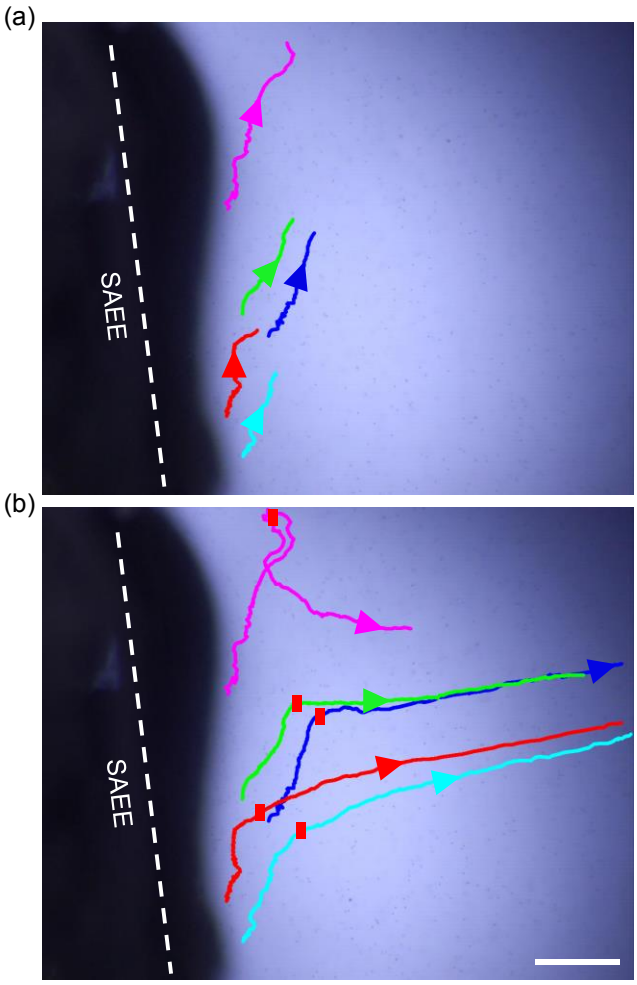


Fig. 5. Trajectories of tracked microparticles before and after turning on the PZT. (a) Motion before PZT activation; directions are denoted by arrows. (b) Motion after PZT activation; the position and orientation of the PZT was kept constant, as denoted by the white dotted line. SAEE denotes the soft acoustic end-effector. Red marks show microparticle positions when the PZT was activated. Scale bar, 500 μm.

references [38]–[40].

## III. Experiments and Results

### A. Experimental setup

The PZT is mounted on the end of the soft robotic arm to obtain the entire soft acoustic end-effector. As shown in Fig. 4, the SAEE is attached to the side of a water tank that is filled with a solution of polystyrene microparticles (with a diameter of 10 μm). Then, the entire setup is mounted under a microscope (Science DST-0745, Bresser). During experiments, the soft robotic arm is actuated using three syringes as described above. The PZT is controlled with a function generator (AFG3011C, Tektronix). The acoustic excitation frequency is around the natural frequency of the PZT (5.5 MHz). The acoustic excitation voltage ranges from 10 $V_{PP}$ to 30 $V_{PP}$. Multi-types of PZTs and various acoustic excitation parameters can be utilized depending on subsequent tasks. The particle trajectory is observed and recorded with a digital camera (DS126281, Canon) and a 0.5x lens. Video analysis is performed using the analytical tools in ImageJ [41].

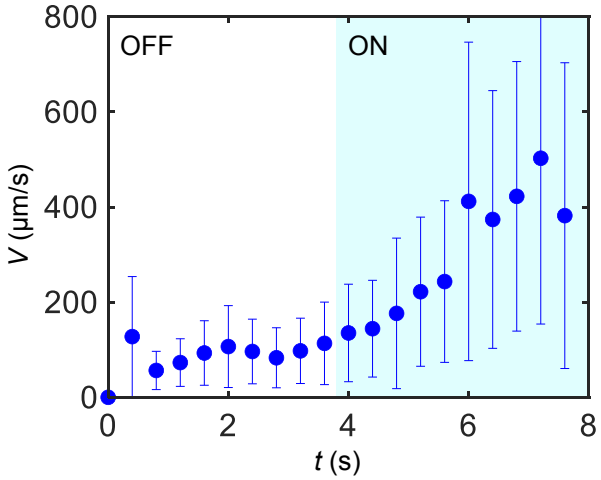


Fig. 6. Plot shows the moving velocity of microparticles against the acoustic excitation. Point denotes the average velocity. The error bar denotes the standard deviation. The PZT was turned on at 3.8 s.

### B. Microparticle manipulation

We first studied the motion of microparticles before and after PZT excitation while holding the position of the PZT constant. As depicted in Fig. 5a and Movie S2, before turning on the PZT, particles moved toward the top-left. It is expected that inhomogeneous particle concentration and complex fluid disturbances cause arbitrary particle motion in the entire bulk solution. In contrast, when the PZT was activated with a square wave at an excitation voltage of 20 $V_{PP}$ and frequency of 5.52 MHz, particles in front of the transducer immediately changed their directions of motion. As shown by the tracked trajectory in Fig. 5b, they started moving in the direction perpendicular to the transducer. An obvious change in microparticles' trajectories after activation of the PZT can indicate the position and orientation of the developed acoustic traveling wave field. We measured the average velocity of these tracked microparticles. Fig. 6 shows that before the PZT is switched on, the particles have a low velocity which is ~ 100 μm/s; upon turning on the PZT, the velocity increases as time goes due to the development of the acoustic traveling wave field. The maximum velocity and effective moving space of microparticles mainly depend on the acoustic excitation voltage. The large standard deviation comes from the different positions and initial conditions of these measured microparticles.

### C. Dynamic adjustment of the acoustic traveling wave field

We then tested the dynamic adjustment of the acoustic traveling wave field with the designed SAEE. As shown in Fig. 7 and Movie S3, when the PZT was activated with the excitation parameters mentioned above, microparticles were continuously pushed away from the transducer along the direction of wave travel. During the process of bending the soft robotic arm and thus changing the spatial orientation of the PZT, changes in the direction of particle movement were observed. Specifically, the unsettled trajectories shown in Fig. 7b and 7c indicate that the position and orientation of the acoustic traveling wave field is sensitive to the deformation of the soft robotic arm. As the soft robotic arm bent into its final shape with a ~30° angle, the direction of microparticle motion

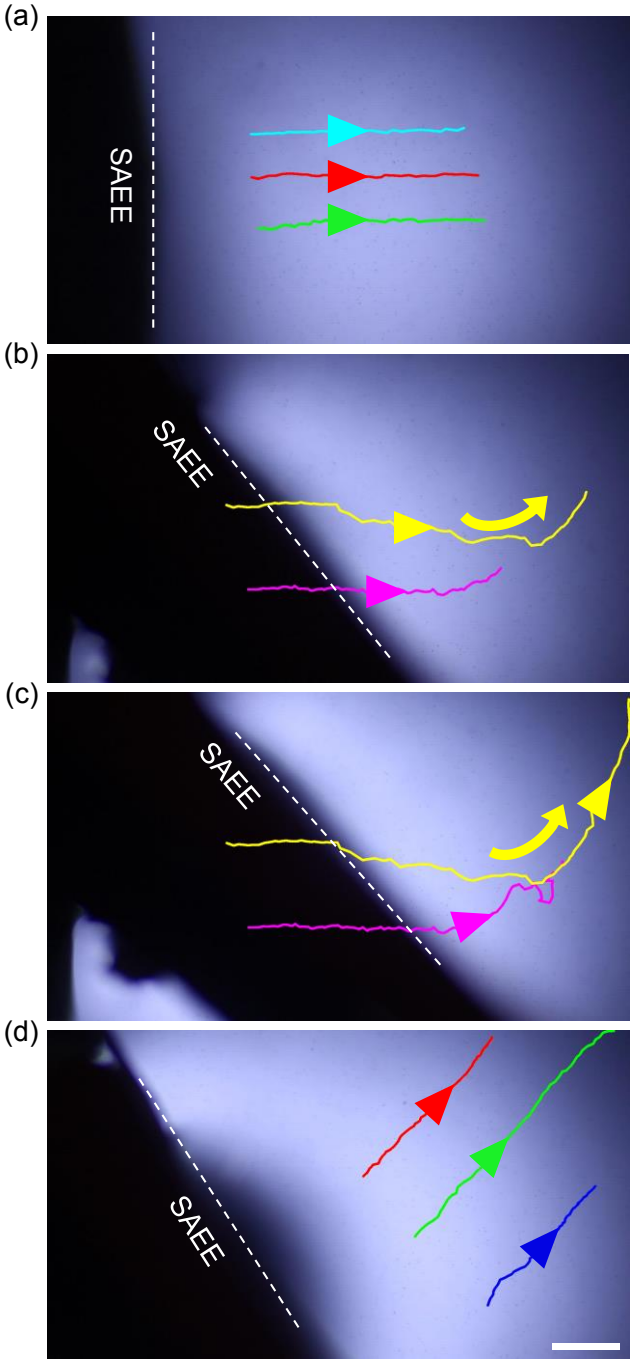


Fig. 7. Dynamic changing of the direction of microparticle motion. (a) When the PZT is positioned vertically, microparticles move along a horizontal trajectory. (b) and (c) While the robotic arm is bending, the microparticle direction is unsettled but echoes the arm's motion. (d) After the arm completes bending, microparticles move at a similar ~30° angle. Yellow arrows denote the direction of microparticle motion. Scale bar, 500 μm.

stabilized at a similar angle (Fig. 7d). Thus, the direction of microparticle motion relies on the position and orientation of the PZT, which is controlled by the deformation of the soft robotic arm. It can be concluded that with programmed pneumatic actuation, more complex and precise microparticle manipulation can be achieved.

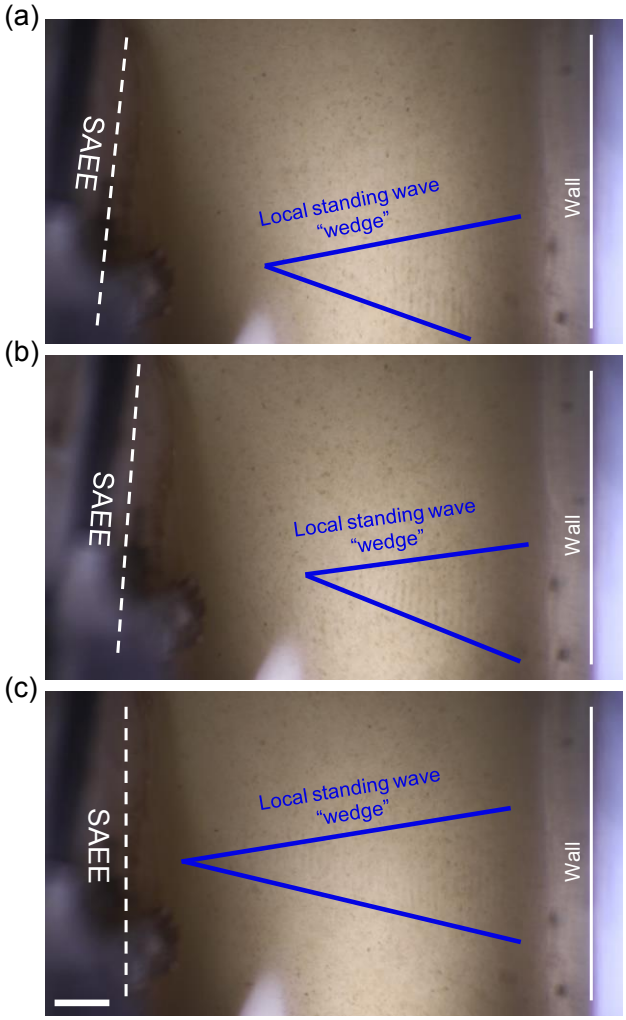


**Fig. 8.** Dynamic acoustic standing wave field modulation. As the PZT is bent to different angles (~6° to ~4° to 0°) by the soft robotic arm, the wedge-shaped standing wave field is developed at different locations. Scale bar, 1 mm.

### *D. Dynamic modulation of the acoustic standing wave field*

To develop an acoustic standing wave field, we moved the SAEE closer to the side boundary of the tank, which functions as an acoustic hard wall and reflects acoustic waves. With a distance of ~9 mm between the PZT and tank wall, we initially excited the PZT with a frequency of 5.52 MHz. Since the formation of a standing wave field requires particular reflection conditions of waves [40], we tuned the frequency until a local standing wave field was achieved. To visualize the pressure nodes of the standing wave field, we used polystyrene microparticles (with a diameter of 3 μm), which have higher density and smaller compressibility relative to water ($\rho_p > \rho_0$ and $k_p < k_0$) and so possess a positive acoustic contrast factor, meaning they will move towards the pressure nodes in the acoustic field. At an acoustic excitation frequency of 5.43 MHz, a homogeneous standing wave field was formed between the wall and the PZT. As evidenced by the visible microparticle lines, the distance between the pressure nodes was 136.38 μm, equaling half of the wavelength.

During subsequent adjustment of the PZT with the soft robotic arm, we observed a local wedge-shaped acoustic

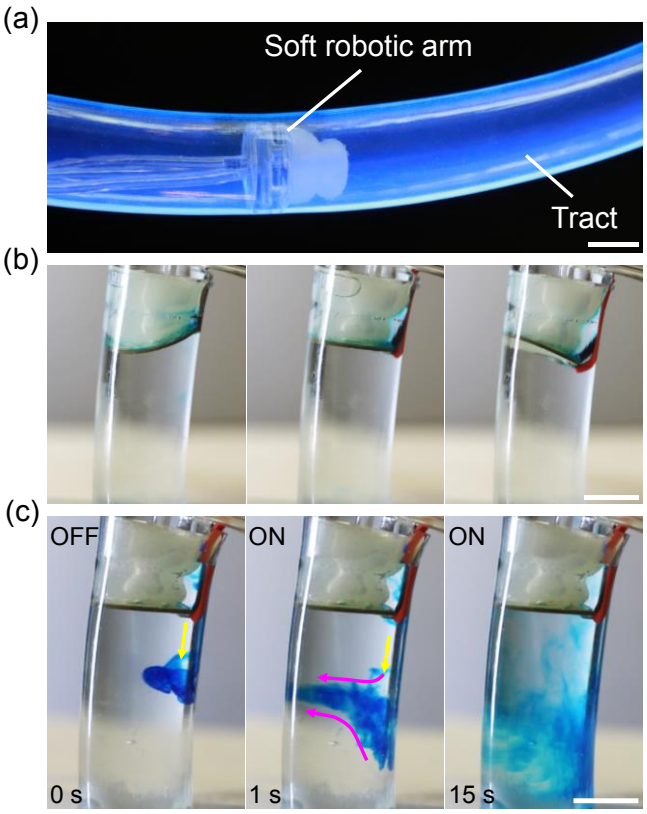


**Fig. 9.** Acoustic micromanipulation in a confined digestive-system-liked tract. (a)The long-distance navigation of the soft robotic arm in the tract. (b)Locally 3D modulation of the SAEE. (C) SAEE controlled acoustic-actuated diffusion. Scale bar, 10 mm.

standing wave field to be developed, as shown in Fig. 8 and Movie S4. It can be inferred that this phenomenon occurs when the PZT is not perfectly parallel to the wall and hence only a small portion of reflected waves intersect the incident waves and form a standing wave. The non-intersected waves act as traveling waves and push microparticles away from the PZT. As the orientation of the SAEE was changed from ~6° to ~4° to 0°, the "wedge" moved along the wall, splitting the flow at different positions. The high precision modulation, ~150 μm per degree, is achieved with a continuous change in position and orientation of the end of the soft robotic arm. In addition, when the three chambers were inflated with equal gas volumes to cause an axial extension of the PZT, the standing wave field disappeared because the distance between the PZT and the wall exceeded that necessary to maintain a standing wave. However, the wave was redeveloped when the soft robotic arm was retracted back. The ability to create and adjust an acoustic standing wave field with micrometer precision proves that this SAEE is a viable tool for target acoustic field modulation.

To further demonstrate the potential applications for *in vivo* acoustic therapies, we manipulated the SAEE in a tract that can mimic the confined human digestive system. Fig. 9a shows that the input pneumatic tubes of the soft robotic arm and the power cables of the PZT can be sorted together behead the SAEE, facilitating long-distance navigation inside the tract. By dynamically adjusting the input gas, the SAEE deforms in 3D space, as shown in Fig.9b, enabling locally multiple-angle acoustic micromanipulation. Fig.9c shows that by stimulating and modulating the SAEE, we could control the diffusion speed and direction of a blue food dye, which was used to represent drugs. Before switching on the PZT, the blue dye fell vertically due to gravity and the effects of liquid diffusion; while under acoustic excitation, the dye began moving horizontally and swiftly dispersed throughout the entire chamber. We believe the SAEE is promising and useful for precise *in vivo* ultrasound-mediated drug release, tissue ablation, organ analysis, and even interrogations at the cellular level.

## IV. Conclusion

In this work, we designed and demonstrated a soft acoustic end-effector that combines a soft robotic arm and a PZT. It is distinct from conventional design paradigms in which the physical position of the PZT is fixed. With pneumatic actuation of the gas chambers inside the soft robotic arm, the position and orientation of the PZT can be adjusted to achieve further acoustic field modulation and microparticle manipulation in an acoustic traveling wave field as well as in an acoustic standing wave field. We optimized the structure of the soft robotic arm to achieve a flat surface during inflation, as illustrated by the simulations. Moreover, we experimentally demonstrated across-scale dynamic acoustic field modulation and microparticle manipulation with micrometer precision in bulk liquid media.

The soft acoustic end-effector is miniature in scale, simple to manufacture, and controllable. It thus blazes a promising trail for flexible and dexterous acoustic applications. In particular, this end-effector opens the door to readily realizing 3D microparticle manipulation. In addition, the cooperative combination of SAEEs can allow multiple types of acoustic fields to be developed. We envision dynamic switching between acoustic fields to follow. Moreover, the SAEE can execute flexible interactions with the human body. As such, it promises to help facilitate efficient and precise acoustic therapy in the future.

## Acknowledgment

D.A. conceived and supervised the project. Z.Z. and M.K. performed experiments and data analysis. Z.Z. and D.A. contributed to the scientific discussion. All authors wrote the manuscript. The authors declare no competing interests.

## References

[1] D. Ahmed, T. Baasch, B. Jang, S. Pane, J. Dual, and B. J. Nelson, "Artificial swimmers propelled by acoustically activated flagella," *Nano Lett.*, vol. 16, no. 8, pp. 4968–4974, 2016.

[2] A. D. C. Fonseca *et al.*, "Ultrasound trapping and navigation of microrobots in the mouse brain vasculature," *Nat. Commun.*, vol. 14, no. 5889, pp. 1–14, 2013.

[3] M. Schrage, M. Medany, and D. Ahmed, "Ultrasound Microrobots with Reinforcement Learning," *Adv. Mater. Technol.*, vol. 8, no. 10, pp. 1–11, 2023.

[4] V. M. Jooss, J. S. Bolten, J. Huwyler, and D. Ahmed, "In vivo acoustic manipulation of microparticles in zebrafish embryos," *Sci. Adv.*, vol. 8, no. 12, pp. 1–10, 2022.

[5] Y. Deng, A. Paskert, Z. Zhang, R. Wittkowski, and D. Ahmed, "An acoustically controlled helical microrobot," *Sci. Adv.*, vol. 9, no. 38, pp. 1–12, 2023.

[6] Z. Zhang, A. Sukhov, J. Harting, P. Malgaretti, and D. Ahmed, "Rolling

microswarms along acoustic virtual walls," *Nat. Commun.*, vol. 13, no. 1, pp. 1–11, 2022.

[7] D. Ahmed *et al.*, "Rotational manipulation of single cells and organisms using acoustic waves," *Nat. Commun.*, vol. 7, no. 11085, pp. 1–11, 2016.

[8] C. Dillinger, N. Nama, and D. Ahmed, "Ultrasound-activated ciliary bands for microrobotic systems inspired by starfish," *Nat. Commun.*, vol. 12, no. 1, pp. 1–11, 2021.

[9] A. Ozcelik *et al.*, "Acoustic tweezers for the life sciences," *Nat. Methods*, vol. 15, no. 12, pp. 1021–1028, 2018.

[10] A. Marzo, S. A. Seah, B. W. Drinkwater, D. R. Sahoo, B. Long, and S. Subramanian, "Holographic acoustic elements for manipulation of levitated objects," *Nat. Commun.*, vol. 6, no. 8661, pp. 1–7, 2015.

[11] J. Shi, X. Mao, D. Ahmed, A. Colletti, and T. J. Huang, "Focusing microparticles in a microfluidic channel with standing surface acoustic waves (SSAW)," *Lab Chip*, vol. 8, no. 2, pp. 221–223, 2008.

[12] M. Wu *et al.*, "Isolation of exosomes from whole blood by integrating acoustics and microfluidics," *Proc. Natl. Acad. Sci. U. S. A.*, vol. 114, no. 40, pp. 10584–10589, 2017.

[13] J. Durrer *et al.*, "A robot-assisted acoustofluidic end effector," *Nat. Commun.*, vol. 13, no. 1, pp. 1–13, 2022.

[14] J. Janiak, Y. Li, Y. Ferry, A. A. Doinikov, and D. Ahmed, "Acoustic microbubble propulsion, train-like assembly and cargo transport," *Nat. Commun.*, vol. 14, no. 1, p. 4705, 2023.

[15] A. Aghakhani, O. Yasa, P. Wrede, and M. Sitti, "Acoustically powered surface-slipping mobile microrobots," *Proc. Natl. Acad. Sci. U. S. A.*, vol. 117, no. 7, pp. 3469–3477, 2020.

[16] J. Rufo, P. Zhang, R. Zhong, L. P. Lee, and T. J. Huang, "A sound approach to advancing healthcare systems: the future of biomedical acoustics," *Nat. Commun.*, vol. 13, no. 1, pp. 1–8, 2022.

[17] T. Xu, L. P. Xu, and X. Zhang, "Ultrasound propulsion of micro-/nanomotors," *Appl. Mater. Today*, vol. 9, pp. 493–503, 2017.

[18] F. W. Liu and S. K. Cho, "3-D swimming microdrone powered by acoustic bubbles," *Lab Chip*, vol. 21, no. 2, pp. 355–364, 2021.

[19] Z. Zhang, Z. Shi, and D. Ahmed, "SonoTransformers: Transformable acoustically activated wireless microscale machines," *Proc. Natl. Acad. Sci. U. S. A.*, vol. 121, no. 6, pp. 1-8, 2024.

[20] Z. Zhang, L. K. Allegrini, N. Yanagisawa, Y. Deng, S. C. F. Neuhauss, and D. Ahmed, "SonoRotor: An Acoustic Rotational Robotic Platform for Zebrafish Embryos and Larvae," *IEEE Robot. Autom. Lett.*, vol. 8, no. 5, pp. 2598–2605, 2023.

[21] P. Agrawal, Z. Zhang, Z. Ghorbanikharaji, Z. Shi, and D. Ahmed, *Acoustic field techniques for cell characterization in health monitoring*. Elsevier Inc., 2023.

[22] F. Hossein, M. Materazzi, P. Lettieri, and P. Angeli, "Application of acoustic techniques to fluid-particle systems – a review," *Chem. Eng. Res. Des.*, vol. 176, pp. 180–193, 2021.

[23] Z. Shi, D. Pu, X. Wang, R. Huan, Z. Jiang, and X. Wei, "Phase-delay induced variation of synchronization bandwidth and frequency stability in a micromechanical oscillator," *Nonlinear Dyn.*, vol. 105, pp. 2981–2994, 2021.

[24] A. Marzo and B. W. Drinkwater, "Holographic acoustic tweezers," *Proc. Natl. Acad. Sci. U. S. A.*, vol. 116, no. 1, pp. 84–89, 2019.

[25] C. Zhong, Y. Jia, D. C. Jeong, Y. Guo, and S. Liu, "Acousnet: A deep learning based approach to dynamic 3d holographic acoustic field generation from phased transducer array," *IEEE Robot. Autom. Lett.*, vol. 7, no. 2, pp. 666-673, 2021.

[26] M. Baudoin, J. C. Gerbedoen, O. B. Matar, N. Smagin, A. Riaud, and J. L. Thomas, "Folding a focalized acoustical vortex on a at holographic transducer: Miniaturized selective acoustical tweezers," *Sci. Adv.*, vol. 5, no. 4, pp. 1–6, 2019.

[27] X. Guo *et al.*, "Acoustofluidic tweezers for the 3D manipulation of microparticles," *IEEE Int. Conf. Robot. Autom.*, pp. 11392–11397, 2020.

[28] H. McClintock, F. Z. Temel, N. Doshi, J. S. Koh, and R. J. Wood, "The milliDelta: A high-bandwidth, high-precision, millimeter-scale Delta robot," *Sci. Robot.*, vol. 3, no. 14, 2018.

[29] M. Leveziel, W. Haouas, G. J. Laurent, M. Gauthier, and R. Dahmouche, "MiGriBot: A miniature parallel robot with integrated gripping for high-throughput micromanipulation," *Sci. Robot.*, vol. 7, no. 69, 2022.

[30] Z. Zhang, X. Wang, S. Wang, D. Meng, and B. Liang, "Design and modeling of a parallel-pipe-crawling pneumatic soft robot," *IEEE Access*, vol. 7, pp. 134301–134317, 2019.

[31] Z. Zhang, X. Wang, H. Liu, B. Liang, and S. Wang, "Kinematic analysis of novel soft robotic arm based on virtual work principle," *IEEE Int. Conf. Robot. Biomimetics*, pp. 984–990, 2018.

[32] Z. Shi, D. Pu, R. Huan, X. Wang, Z. Jiang, and X. Wei, "Mode interaction induced response flattening in two mechanically coupled micro-resonators," *Mechan. Syst. Signal Proc.*, vol. 177, no. 1, pp. 1–11, 2022.

[33] Z. Zhang, X. Wang, D. Meng, and B. Liang, "Bioinspired spiral soft pneumatic actuator and its characterization," *J. Bionic Eng.*, vol. 18, no. 5, pp. 1101–1116, 2021.

[34] Y. Hao et al., "Universal soft pneumatic robotic gripper with variable effective length," *Chinese Control Conf.*, pp. 6109–6114, 2016.

[35] Z. Zhang, S. Wang, D. Meng, X. Wang, and B. Liang, "Soft-CCD Algorithm for Inverse Kinematics of Soft Continuum Manipulators," *IEEE Int. Conf. Intell. Robot. Syst.*, pp. 639–644, 2021.

[36] B. L. V K and M. Physics, "On the acoustic radiation pressure on spheres," *Proc. R. Soc. London. Ser. A - Math. Phys. Sci.*, vol. 147, no. 861, pp. 212–240, 1934.

[37] H. Bruus, "Acoustofluidics 7: the acoustic radiation force on small particles," *Lab Chip*, vol. 12, no. 6, pp. 1014–1021, 2012.

[38] M. Settnes and H. Bruus, "Forces acting on a small particle in an acoustical field in a viscous fluid," *Phys. Rev. E - Stat. Nonlinear, Soft Matter Phys.*, vol. 85, no. 1, pp. 1–12, 2012.

[39] K. Yosioka and Y. Kawasima, "Acoustic radiation pressure on a compressible sphere," *Acta Acust. united with Acust.*, vol. 5, no. 3, pp. 167–173, 1955.

[40] J. Dual and D. Möller, "Acoustofluidics 4: piezoelectricity and application in the excitation of acoustic fields for ultrasonic particle manipulation," *Lab Chip*, vol. 12, no. 3, pp. 506–514, 2012.

[41] C. A. Schneider, W. S. Rasband, and K. W. Eliceiri, "NIH image to ImageJ: 25 years of image analysis," *Nat. Methods*, vol. 9, no. 7, pp. 671–675, 2012.